Materials Advances

ROYAL SOCIETY OF CHEMISTRY

PAPER

View Article Online
View Journal | View Issue

Cite this: *Mater. Adv.*, 2023, 4, 1927

6*H*-[1,2,5]Thiadiazolo[3,4-*e*]thieno[3,2-*b*]indole-flanked *para*-azaquinodimethane based aromatic-quinoidal polymer semiconductors with high molecular weights synthesized *via* direct arylation polycondensation†

Yufa Xiao,[a] Huaijie Fu,[b] Zefeng Li,[a] Yingxuan Zheng,[a] Ping Deng, *[a] Yanlian Lei *[b] and Yan Yu*[a]

Received 18th January 2023,
Accepted 15th March 2023

DOI: 10.1039/d3ma00037k

rsc.li/materials-advances

The 6*H*-[1,2,5]thiadiazolo[3,4-*e*]thieno[3,2-*b*]indole-flanked *para*-azaquinodimethane (*p*-AQM)-based polymer semiconductors **PQ-1** and **PQ-2** are rationally designed through a π-extended aromatic-quinoidal design strategy. They are synthesized by the direct arylation polycondensation (DArP) method. Their physicochemical properties are investigated. Both polymers show high number-average molecular weights of over 120 kDa. **PQ-1** exhibits a narrower band gap compared to its thiophene-flanked *p*-AQM polymer counterpart. **PQ-2**, with more aromatic thiophene units in the conjugated main chains, displays a broader band gap compared to **PQ-1**. Both **PQ-1** and **PQ-2** possess high-lying highest occupied molecular orbital energy levels (about −5.0 eV). They exhibit typical p-type semiconductor characteristics according to the results of characterization of organic field-effect transistors. This work presents an alternative π-extended aromatic-quinoidal design strategy and a convenient DArP method to build new *p*-AQM polymer semiconductors.

1. Introduction

Polymer semiconductors have received significant attention because they possess broad application prospects in organic electronics, such as organic field effect transistors (OFETs).[1–5] In addition to that of conventional aromatic conjugated polymers, rapid progress in the development of conjugated polymers with quinoidal structures has been noted in recent years.[6–9] The interest in the field is being increased because of the possibility of creating conjugated systems that combine the unique properties of aromatic and quinoidal moieties.[10–14] The introduction of quinoidal units into the polymer backbones can effectively tune the physicochemical properties of the resulting polymers.[15–17]

Recently, Liu and co-workers have developed a promising *para*-azaquinodimethane (*p*-AQM) building block, which features an *N*-heteroaromatic quinoidal skeleton and has the ability to stabilize the quinoidal character of the conjugated system.[18] The reported thiophene-flanked *p*-AQMs, which possess a coplanar structure and rigid conformation with limited rotational freedom due to non-covalent intramolecular S···N interactions, have generated significant interest in functional polymeric materials.[18,19] The thiophene-flanked *p*-AQMs also exhibit distinct advantages of facile synthesis, ease of insertion into polymer backbones, and flexible band gap engineering.[20,21] The fused heteroaromatic conjugated materials have been widely proven to be promising semiconducting small molecules[22–28] and polymers.[29–33] As a linked unit in the conjugated polymer, replacing the single thiophene ring with the fused heteroaromatic ring endows the resulting polymer with tunable physicochemical and semiconducting properties.[34–36] For example, introducing the benzo[*c*][1,2,5]thiadiazole unit into a thiophene-flanked *p*-AQM polymer backbone offers improved backbone rigidity, stronger intermolecular interactions, and higher crystallinity, endowing the resulting polymer with high hole transport mobility.[37] Therefore, the introduction of the fused heteroaromatic rings in *p*-AQMs may further expand the molecular design strategies of *p*-AQM-based conjugated polymers. However, the

[a] *Key Laboratory of Advanced Materials Technologies, International (HongKong Macao and Taiwan) Joint Laboratory on Advanced Materials Technologies, College of Materials Science and Engineering, Fuzhou University, Fuzhou, Fujian, 350108, China. E-mail: pingdeng@fzu.edu.cn, yuyan@fzu.edu.cn*

[b] *School of Physical Science and Technology, Chongqing Key Lab of Micro&Nano Structure Optoelectronics, Southwest University, Chongqing 400715, China. E-mail: yllei@swu.edu.cn*

† Electronic supplementary information (ESI) available. See DOI: https://doi.org/10.1039/d3ma00037k

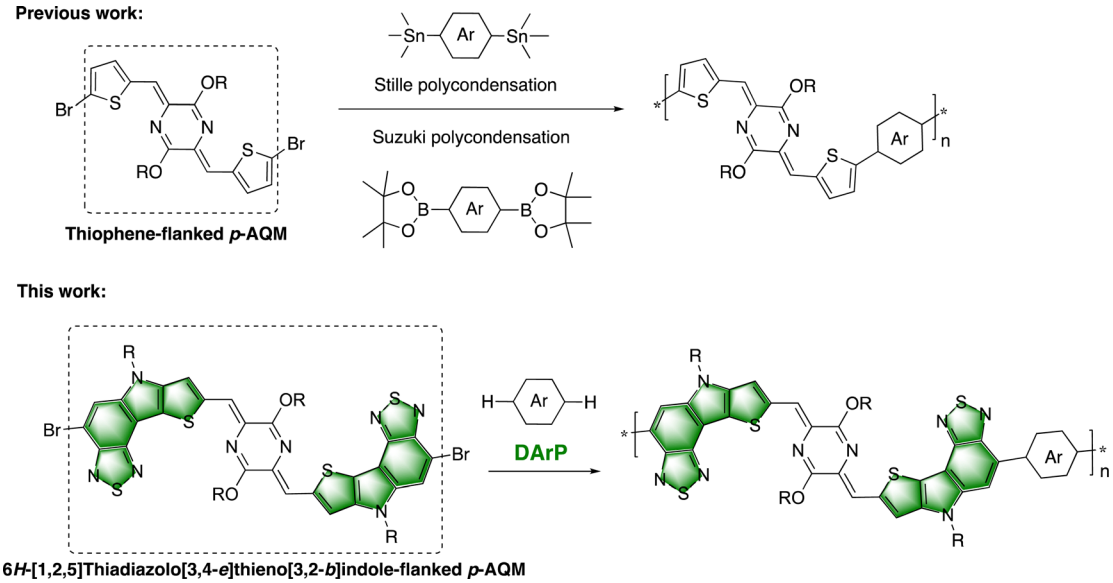

Fig. 1 Design strategies for *p*-AQM conjugated polymers.

utilization of fused heteroaromatic ring-flanked *p*-AQMs for building conjugated polymers remains unexplored.

Another significant consideration for building *p*-AQM-based polymers is the choice of polymerization method. This kind of conjugated polymer has been still prepared by traditional Stille or Suzuki polycondensations (Fig. 1). The requisite organotin or organoboron monomers represent the limitations of reactions in terms of atom economy and green synthesis. It is encouraging that direct arylation polymerization has become a promising method for preparing conjugated polymers.[38–47] However, it is still challenging to achieve solution-processed conjugated polymers with high molecular weights (M_n > 100 kDa).[38–50]

In this work, we present an alternative molecular design and synthetic strategy of *p*-AQM conjugated polymers (Fig. 1). A new fused heteroaromatic ring-flanked *p*-AQM monomer has been synthesized based on the 6*H*-[1,2,5]thiadiazolo[3,4-*e*]thieno[3,2-*b*]indole building block. This unique monomer has been further introduced into the backbones of *p*-AQM polymers through the convenient DArP method with thiophene-based units as the comonomers. The physicochemical properties and charge transport properties of the resulting polymers (**PQ-1** and **PQ-2**) have been investigated.

2. Results and discussion

Design, theory calculations, and synthesis

In terms of bromo-6*H*-[1,2,5]thiadiazolo[3,4-*e*]thieno[3,2-*b*]-indole (TTI), it is an asymmetric conjugated building unit constructed through the *N*-bridging strategy of a thiophene and benzo[*c*][1,2,5]thiadiazole. The TTI-flanked *p*-AQM is the target monomer **M**. The long, branched decyl tetradecyl side chains were employed on the periphery of **M** to support the solubility of its polymers. The density functional theory (DFT) calculation (B3LYP-D/6-31G(d) level) of **M** was carried out and the resulting optimized conformation is shown in Fig. 2. The dihedral angle between TT1 and *p*-AQM was 0.2°, indicating the planarity of the conjugated backbone. The synthetic route of the monomer **M** is shown in Scheme 1. Compound **1** was prepared according to the reported procedure.[51] The Stille coupling reaction of compound **1** and tributyl(thiophen-2-yl)stannane provided compound **2** with a yield of 87%. The intermediate **3** was then prepared *via* Cadogan cyclization and following *N*-alkylation reactions in a total yield of 43%. The Vilsmeier–Haack reaction of intermediate **3** yielded intermediate **4** with a yield of 88%. Monomer **M** was obtained by Knoevenagel condensation between 1,4-diacetyl-2,5-diketopiperazine and intermediate **4** and subsequent alkylation in the presence of K_2CO_3 in a total yield of 48%. It should be noted that the O-alkylated product was gained rather than the *N*-alkylated one because a tautomerization occurs upon deprotonation of the amide.[18–21] The structure of monomer **M** was assigned by nuclear magnetic resonance, high-resolution mass spectrometry, and infrared spectroscopy (see ESI†).

With monomer **M** in hand, the 2,2′-bithiophene and 2,5-dithiophen-2-ylthieno[3,2-*b*]thiophene units were employed as

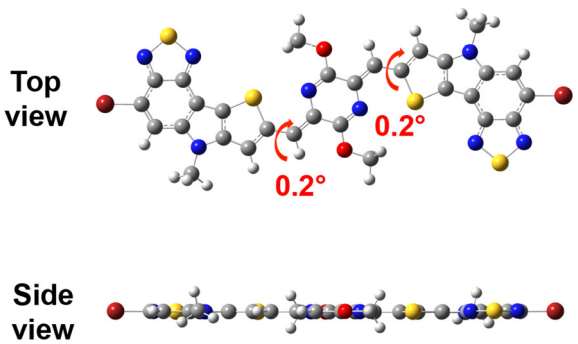

Fig. 2 Optimized molecular geometry of **M**. Alkyl chains were replaced with methyl groups for simplification.

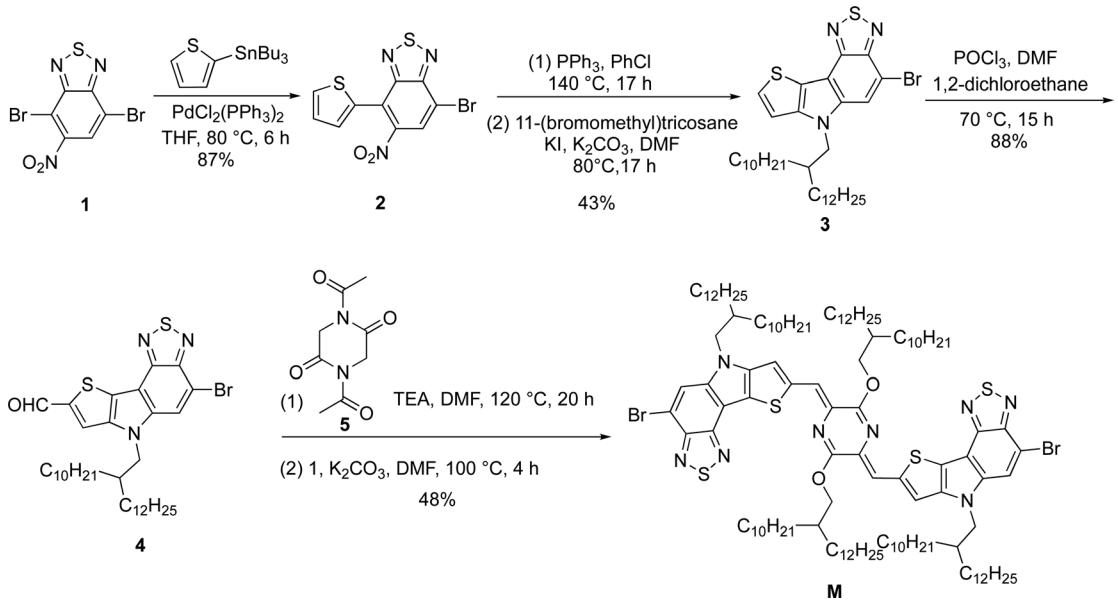

Scheme 1 Synthesis of the monomer **M**.

comonomers to build aromatic-quinoidal conjugated polymers (**PQ-1** and **PQ-2**) using DArP methods, respectively. The optimized conformation of the repeating units of target polymers **PQ-1** and **PQ-2** are shown in Fig. 3. The calculated results showed that they possessed similar calculated orbital electron distribution and energy levels. The model molecules with 2,2′-bithiophene and 2,5-di(thiophen-2-yl)thieno[3,2-*b*]thiophene bridge units were also calculated. The results showed that they owned relatively good conjugated backbone planarity (Fig. S19, ESI†). Synthetic routes to the polymers are shown in Scheme 2. The detailed synthetic procedures and characterizations are depicted in the ESI.† **PQ-1** and **PQ-2** were synthesized using Pd-catalyzed DArP of the monomer **M** and the corresponding comonomers 2,2′-bithiophene and 2,5-di(thiophen-2-yl)thieno[3,2-*b*]thiophene, respectively. The yield of **PQ-1** can reach 96%, while that of **PQ-2** was only 44%. The polymerization reaction of **M** and 2,5-dithiophen-2-ylthieno[3,2-*b*]thiophene produced an insoluble solid (yield: 46%), meaning that the synthetic yield for **PQ-2** is low. It is possible that the 2,5-di(thiophen-2-yl)thieno[3,2-*b*]thiophene has more beta-protons, and the polymerization to give **PQ-2** may have produced more branched structures with partial crosslinking. The polymer **PQ-1** displayed good solubilities in tetrahydrofuran, toluene, chloroform and chlorobenzene, and the concentration of the polymer could reach 20 mg mL^{-1}. **PQ-2** could only be dissolved in chlorinated solvents, such as chloroform and chlorobenzene, and the concentration of the polymer was less than 10 mg mL^{-1}. The thermogravimetric analysis showed that the temperature of 5% thermal weight loss of **PQ-1**

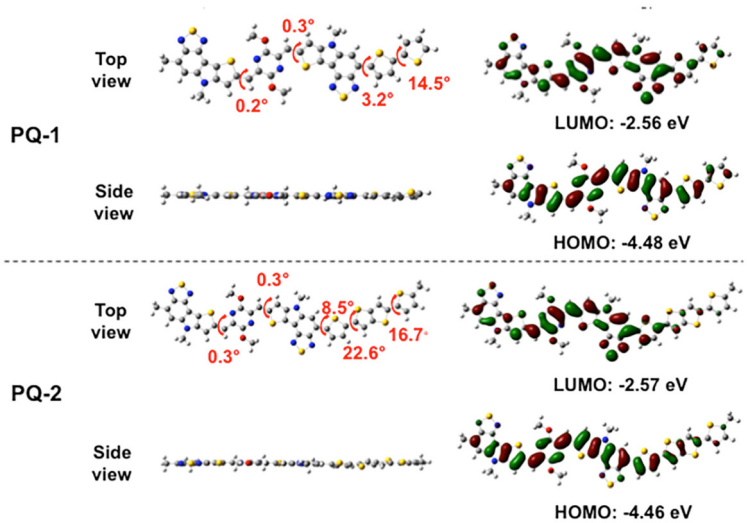

Fig. 3 Optimized geometry, electron cloud distribution, and molecular orbital energy levels of repeating units of **PQ-1** and **PQ-2**. Alkyl chains were replaced with methyl groups for simplification.

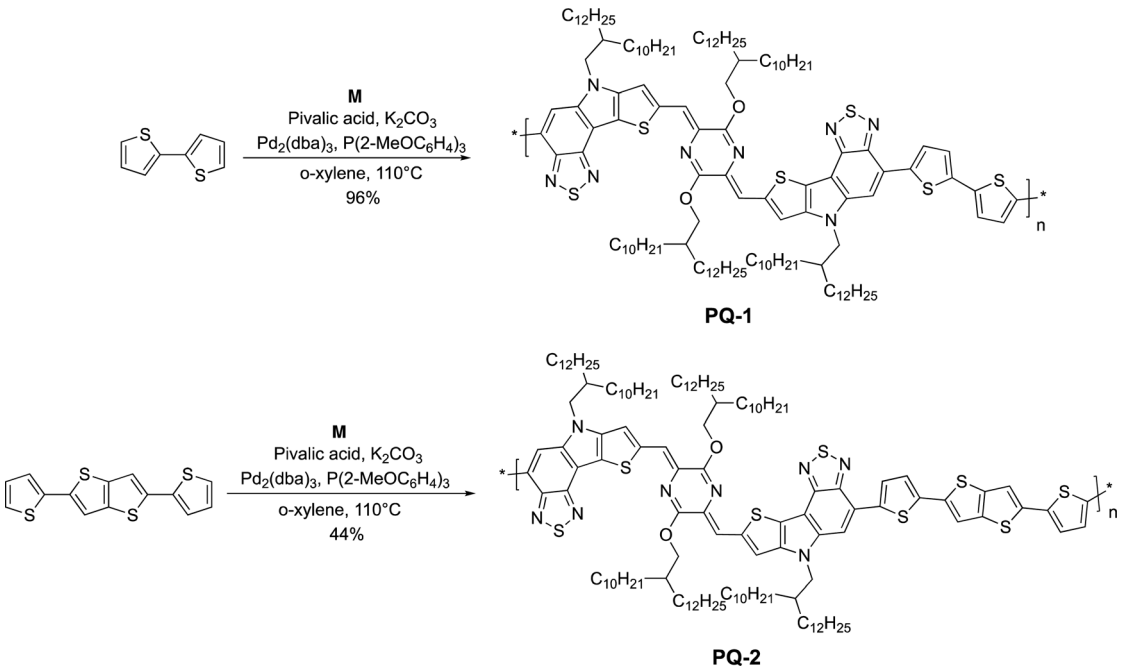

Scheme 2 Synthesis of the polymers **PQ-1** and **PQ-2**.

Table 1 Molecular weights and polydispersity index ($Đ$) of **PQ-1** and **PQ-2**

Polymer	M_n (kDa)	M_w (kDa)	$Đ$
PQ-1	155.7	426.5	2.74
PQ-2	128.3	311.7	2.43

and **PQ-2** was above 380 °C, indicating good thermal stability (Fig. S15, ESI†). Similar to some thiophene-flanked *p*-AQM-based polymers,[20] **PQ-1** and **PQ-2** showed no obvious phase-transition peaks in the range of 50 to 300 °C. The molecular weights of both polymers were evaluated through high-temperature GPC working at 150 °C. The number-average molecular weights (M_n) of **PQ-1** and **PQ-2** were calculated to be 155.7 and 128.3 kDa with a dispersity of 2.74 and 2.43, respectively (Table 1 and Fig. S13 and S14, ESI†). To the best of our knowledge, they have the highest molecular weight of this class of *p*-AQM conjugated polymers.

Optical and electrochemical properties

The optical properties of **M**, **PQ-1**, and **PQ-2** were investigated by UV-vis absorption spectroscopy (Fig. 4). **M** was compared to the known thiophene-flanked *p*-AQM monomer **M-ref**[18] (see Fig. S17, ESI†). The UV-vis absorption spectra of **M-ref** are depicted in Fig. S17 (ESI†). The **M-ref** in a dilute chloroform solution showed an absorption maximum at 452 nm, which could be attributed to a π–π* transition. Unlike **M-ref**, **M** in the dilute chloroform solution showed an absorption spectrum with two well-resolved peaks at 564 and 610 nm, which could be attributed to the extension of the π-conjugated system, and intramolecular charge transfer caused by brominated 6*H*-[1,2,5]thiadiazolo[3,4-*e*]thieno[3,2-*b*]indole moieties located at the two ends of molecule **M**. The molar extinction coefficient for the primary absorption of **M** was four times that of **M-ref** (Fig. 3a and Fig. S18 (ESI†) and Table 2). In the thin film, the maximum absorption value of **M-ref** showed little difference from that of **M-ref** in the dilute chloroform solution, but a broader absorption spectrum. However, **M** showed a distinct blue-shift in maximum absorption (~536 nm) compared to its solution, which could be attributed to H-aggregations.[52,53] Compared with **M**, **M**-based polymers **PQ-1** and **PQ-2** possessed significantly red-shifted adsorption spectra. Both polymer solutions had high molar extinction coefficients in the visible-light region (Fig. 3a). Both polymer thin films showed broader absorption characteristics as compared with those of their corresponding solutions, indicating stronger interchain interaction in the solid state. The maximum absorption values of the **PQ-1** and **PQ-2** thin films were 768 and 672 nm, respectively. The optical band gaps of the thin films estimated from the absorption onsets for **PQ-1** and **PQ-2** were 1.45 and 1.54 eV, respectively. Compared to the **PQ-2** thin film, the **PQ-1** thin film had more red-shifted absorption and a narrower band gap. The thiophene-flanked *p*-AQM and 2,2′-bithiophene-based polymer **PQ-ref**[18] (see Fig. S17, ESI†) was chosen as the reference polymer. Compared to **PQ-ref**, the 6H-[1,2,5]thiadiazolo[3,4-*e*]thieno[3,2-*b*]indole-flanked and *p*-AQM and 2,2′-bithiophene-based polymer **PQ-1** showed a narrower band gap (Table 2).

The electrochemical energy levels of **M**, **M-ref**, **PQ-1**, and **PQ-2** thin films were evaluated using cyclic voltammetry. The cyclic voltammogram is presented in Fig. 5a. The highest occupied molecular orbital energy levels (E_{HOMO}) and lowest unoccupied molecular orbital energy levels (E_{LUMO}) of each sample were estimated from their respective onset oxidations (E_{ox}) and onset reductions (E_{red}), respectively. The data are shown in Fig. 5b and Table 3. **M** had a similar E_{LUMO} compared to **M-ref** but slightly lower E_{HOMO} (−5.19 *vs.* −5.14 eV). **PQ-1** and **PQ-2** possessed

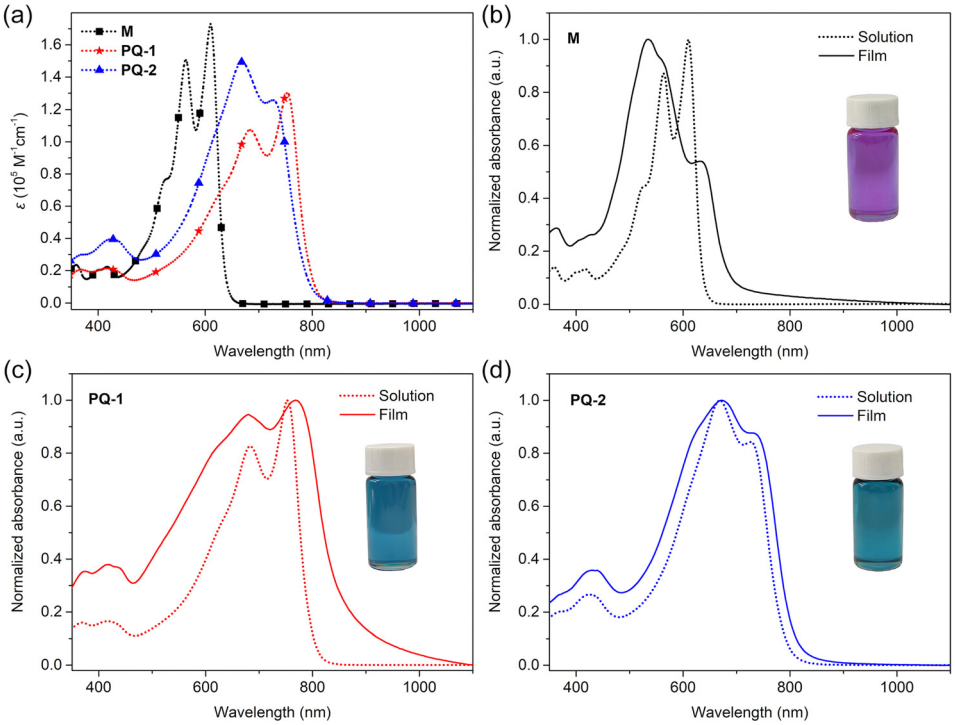

Fig. 4 (a) UV-vis absorption spectra of the chlorobenzene solutions of **M**, **PQ-1** and **PQ-2**; (b–d) Normalized UV-vis absorption spectra of the chlorobenzene solutions and thin films of **M**, **PQ-1** and **PQ-2**.

Table 2 Optical properties of the monomers and polymers

Material	ε [10^5 $M^{-1}cm^{-1}$]	$\lambda_{max}^{solution a}$ [nm]	$\lambda_{onset}^{solution}$ [nm]	λ_{max}^{film} [nm]	λ_{onset}^{film} [nm]	$E_g^{opt b}$ [eV]
M	1.7	564, 610	635	536, 632	685	1.81
M-ref	0.4	452	492	450	498	2.49
PQ-1	1.5	684, 752	793	680, 768	858	1.45
PQ-2	1.3	668, 728	787	672, 736	805	1.54
PQ-ref[18]	0.85	731	805	731	810	1.53

[a] Measured in chlorobenzene. [b] Calculated by the equation: $E_g^{opt} = 1240/\lambda_{onset}^{film}$ (eV).

similar E_{HOMO} values, slightly higher than the reference polymer **PQ-ref**[18] (see Fig. S17, ESI†). The results were consistent with the theoretical calculation. The electrochemical energy levels of **PQ-1** and **PQ-2** indicated that both polymers could be potential hole transport materials.

Charge transport properties

The OFETs with a bottom-gate top-contact device configuration were fabricated to investigate the charge-transport properties of **PQ-1** and **PQ-2**. Fig. 6a–d show the transfer characteristics and

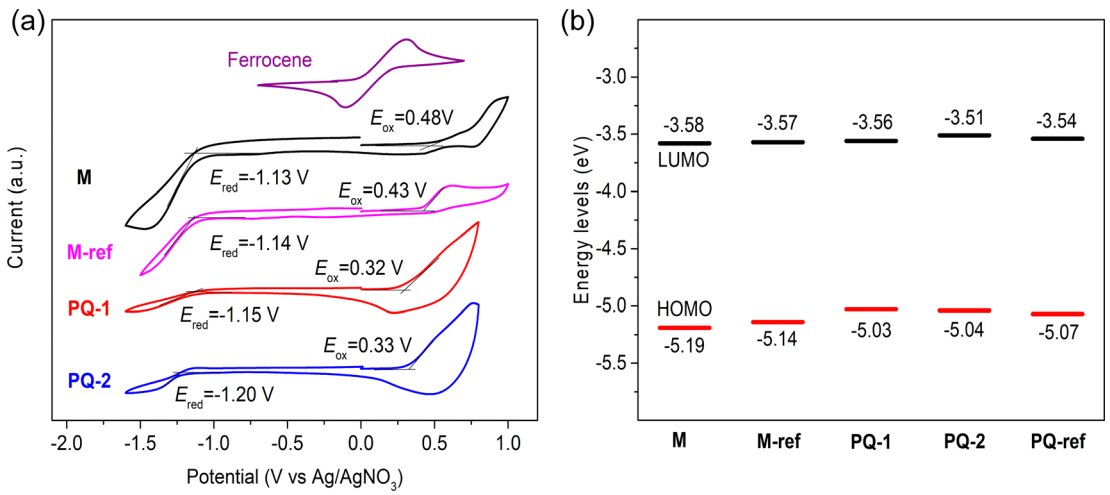

Fig. 5 (a) Cyclic voltammogram of monomers and polymers and (b) energy level diagram of the monomers and polymers.

Table 3 Electrochemical properties of **M**, **M-ref**, **PQ-1**, **PQ-2** and **PQ-ref**

Material	E_{red} [V]	E_{LUMO}[a] [eV]	E_{ox} [V]	E_{HOMO}[b] [eV]
M	−1.13	−3.58	0.48	−5.19
M-ref	−1.14	−3.57	0.43	−5.14
PQ-1	−1.15	−3.56	0.32	−5.03
PQ-2	−1.20	−3.51	0.33	−5.04
PQ-ref[18]	-	−3.54	0.27	−5.07

[a] $E_{LUMO} = -(E_{red} - E_{1/2}^{Fc/Fc+} + 4.8)$ eV, $E_{1/2}^{Fc/Fc+} = 0.09$ V. [b] $E_{HOMO} = -(E_{ox} - E_{1/2}^{Fc/Fc+} + 4.8)$ eV.

corresponding $|I_{DS}|^{1/2}$-V_G curves of the six separated OFET devices for **PQ-1** and **PQ-2** in one batch, respectively, which reflects the relatively good uniformity and repeatability based on **PQ-2**. The representative output characteristics of OFETs based on **PQ-1** and **PQ-2** are shown in Fig. 6e and f, respectively. Both polymers showed p-type transport with a hole mobility of $\sim 10^{-3}$ cm^2 V^{-1} s^{-1} and current on/off ratio (I_{on}/I_{off}) $>10^3$ (Table 4), comparable to the hole mobility of the as-cast **PQ-ref** film reported in the literature.[18] The as-cast films of both polymers showed only (100) diffraction peaks in their X-ray

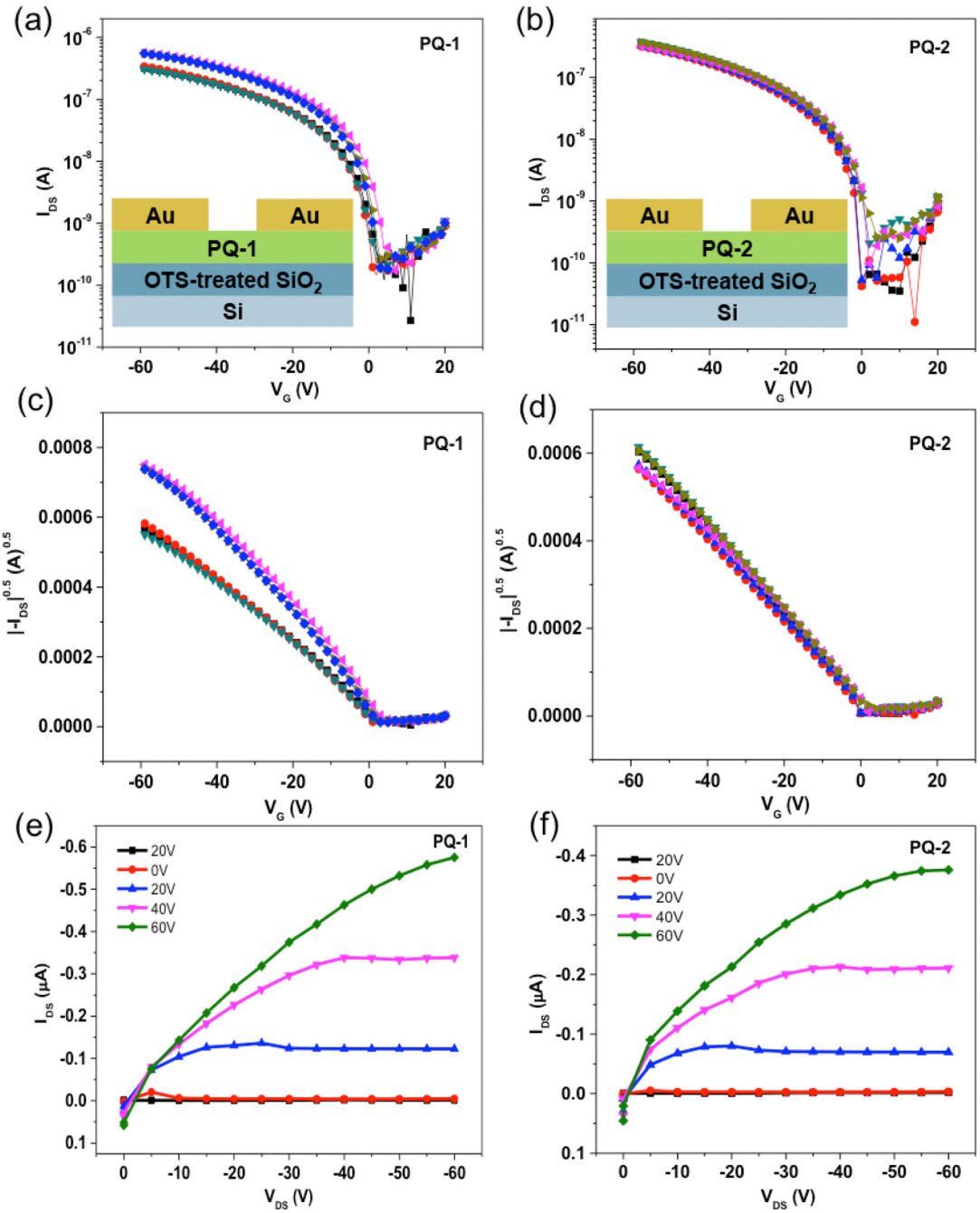

Fig. 6 (a) Transfer, (c) $|I_{DS}|^{1/2}$-V_G, and (e) output curves of OFETs based on **PQ-1**; (b) transfer, (d) $|I_{DS}|^{1/2}$-V_G and (f) output curves of OFETs based on **PQ-2**.

Table 4 OFET performance of **PQ-1** and **PQ-2**[a]

Polymer	μ_h [$cm^2 V^{-1} s^{-1}$]	I_{on}/I_{off}	V_T [V]
PQ-1 (at cast)	2.0×10^{-3}	2.9×10^3	2.8
PQ-2 (at cast)	1.3×10^{-3}	1.0×10^3	1.1

[a] Average performance parameters of six devices.

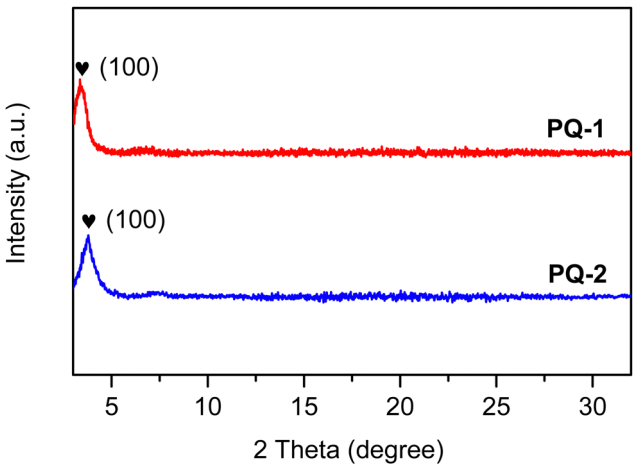

Fig. 7 X-ray diffraction patterns of **PQ-1** and **PQ-2**.

diffraction (XRD) spectra, indicating that they possessed low crystallinity to some extent (Fig. 7).

Conclusions

In summary, we have designed and synthesized two new 6*H*-[1,2,5]thiadiazolo[3,4-*e*]thieno[3,2-*b*]indole-flanked *p*-AQM based aromatic-quinoidal polymer semiconductors **PQ-1** and **PQ-2**. To the best of our knowledge, these are the first *p*-AQM polymers synthesized by the convenient DArP method. Both polymers had high molecular weights (M_n > 120 kDa) and low band gaps (E_g < 1.55 eV). Compared to the reference polymer **PQ-ref**, **PQ-1** with the same electron donor unit had more red-shifted absorption. Similarly to **PQ-ref**, **PQ-1** and **PQ-2** possessed a high E_{HOMO} (~−5.0 eV) and displayed typical p-type transport properties. We expect that the design strategy to flank fused heteroaromatic rings and the DArP method possess excellent potential to develop new π-extended conjugated unit-based polymer semiconductors.

Conflicts of interest

The authors declare no competing financial interest.

Acknowledgements

This work was financially supported by the National Natural Science Foundation of China (No. 21704015, U1905215, and 52072076), the Natural Science Foundation of Fujian Province (2021J01596), and the Natural Science Foundation Project of CQ CSTC (cstc2020jcyj-msxmX0488).

Notes and references

1 X. Guo and A. Facchetti, *Nat. Mater.*, 2020, **19**, 922–928.
2 F. Huang, Z. S. Bo, Y. H. Geng, X. H. Wang, L. X. Wang, Y. G. Ma, J. H. Hou, W. P. Hu, J. Pei, H. L. Dong, S. Wang, Z. Li, Z. G. Shuai, Y. F. Li and Y. Cao, *Acta Polym. Sin.*, 2019, **50**, 988–1046.
3 S. Holliday, J. E. Donaghey and I. McCulloch, *Chem. Mater.*, 2014, **26**, 647–663.
4 W. V. Wang, Y. Zhang, X.-Y. Li, Z.-Z. Chen, Z.-H. Wu, L. Zhang, Z.-W. Lin and H.-L. Zhang, *InfoMat*, 2021, **3**, 814–822.
5 Y. Yang, Z. Liu, G. Zhang, X. Zhang and D. Zhang, *Adv. Mater.*, 2019, **31**, 1903104.
6 X. Zhao, H. Cai, Y. Deng, Y. Jiang, Z. Wang, Y. Shi, Y. Han and Y. Geng, *Macromolecules*, 2021, **54**, 3498–3506.
7 T. Mikie, M. Hayakawa, K. Okamoto, K. Iguchi, S. Yashiro, T. Koganezawa, M. Sumiya, H. Ishii, S. Yamaguchi, A. Fukazawa and I. Osaka, *Chem. Mater.*, 2021, **33**, 8183–8193.
8 C. L. Anderson, N. Dai, S. J. Teat, B. He, S. Wang and Y. Liu, *Angew. Chem., Int. Ed.*, 2019, **58**, 17978–17985.
9 J. Huang and G. Yu, *Mater. Chem. Front.*, 2021, **5**, 76–96.
10 T. Du, Y. Liu, C. Wang, Y. Deng and Y. Geng, *Macromolecules*, 2022, **55**, 5975–5984.
11 P. Deng, L. Liu, S. Ren, H. Li and Q. Zhang, *Chem. Commun.*, 2012, **48**, 6960–6962.
12 Y. Deng, B. Sun, Y. He, J. Quinn, C. Guo and Y. Li, *Angew. Chem., Int. Ed.*, 2016, **55**, 3459–3462.
13 C. Dong, Bi Meng, J. Liu and L. Wang, *J. Mater. Chem. C*, 2022, **10**, 2718–2723.
14 S. Dong and Z. Li, *J. Mater. Chem. C*, 2022, **10**, 2431–2449.
15 T. Mikie and I. Osaka, *J. Mater. Chem. C*, 2020, **8**, 14262–14288.
16 X. Ji and L. Fang, *Polym. Chem.*, 2021, **12**, 1347–1361.
17 M. Yang, T. Du, X. Zhao, X. Huang, L. Pan, S. Pang, H. Tang, Z. Peng, L. Ye, Y. Deng, M. Sun, C. Duan, F. Huang and Y. Cao, *Sci. China: Chem.*, 2021, **64**, 1219–1227.
18 X. Liu, B. He, C. L. Anderson, J. Kang, T. Chen, J. Chen, S. Feng, L. Zhang, M. A. Kolaczkowski, S. J. Teat, M. A. Brady, C. Zhu, L.-W. Wang, J. Chen and Y. Liu, *J. Am. Chem. Soc.*, 2017, **139**, 8355–8363.
19 X. Liu, B. He, A. Garzón-Ruiz, A. Navarro, T. L. Chen, M. A. Kolaczkowski, S. Feng, L. Zhang, C. A. Anderson, J. Chen and Y. Liu, *Adv. Funct. Mater.*, 2018, **28**, 1801874.
20 H. Liang, C. Liu, Z. Zhang, X. Liu, Q. Zhou, G. Zheng, X. Gong, L. Xie, C. Yang, L. Zhang, B. He, J. Chen and Y. Liu, *Adv. Funct. Mater.*, 2022, **32**, 2201903.
21 B. Dyaga, S. Mayarambakam, O. A. Ibraikulov, N. Zimmermann, S. Fall, O. Boyron, T. Heiser, N. Leclerc, N. Berton and B. Schmaltz, *Mater. Adv.*, 2022, **3**, 6853–6861.
22 C. Chen, C.-Z. Du and X.-Y. Wang, *Adv. Sci.*, 2022, **9**, 2200707.
23 H. Xin, B. Hou and X. Gao, *Acc. Chem. Res.*, 2021, **54**, 1737–1753.
24 N. Liang, D. Meng and Z. Wang, *Acc. Chem. Res.*, 2021, **54**, 961–975.
25 Y. Ma, D. Cai, S. Wan, P. Wang, J. Wang and Q. Zheng, *Angew. Chem., Int. Ed.*, 2020, **59**, 21627–21633.
26 J. Guo, Y. Yang, C. Dou and Y. Wang, *J. Am. Chem. Soc.*, 2021, **143**, 18272–18279.

27 H. Jiang, S. Zhu, Z. Cui, Z. Li, Y. Liang, J. Zhu, P. Hu, H.-L. Zhang and W. Hu, *Chem. Soc. Rev.*, 2022, **51**, 3071–3122.
28 W. Xia, Y. Huang, P. Deng and Y. Yu, *Dyes Pigm.*, 2022, **208**, 110825.
29 Z.-F. Yao, Y.-Q. Zheng, J.-H. Dou, Y. Lu, Y. Ding, L. Ding, J.-Y. Wang and J. Pei, *Adv. Mater.*, 2021, **33**, 2006794.
30 B. Liu, J. Li, W. Zeng, W. Yang, H. Yan, D.-C. Li, Y. Zhou, X. Gao and Q. Zhang, *Chem. Mater.*, 2021, **33**, 580–588.
31 X. Tao, Y. Liu, L. Du, Y. Yan, Z. Wu, Y. Zhao, Y. Guo, H. Chen and Y. Liu, *J. Mater. Chem. C*, 2021, **9**, 15083–15094.
32 D.-W. Liu, Y. Zhang, X.-Y. Li, Q. Xiao, W.-J. Sun, X. Shao and H.-L. Zhang, *J. Mater. Chem. C*, 2021, **9**, 6560–6567.
33 R. C. L. Gott-Betts, A. A. Burney-Allen, D. L. Wheeler and M. Jeffries-EL, *Mater. Adv.*, 2022, **3**, 4831–4838.
34 J. Ji, X. Wu, P. Deng, D. Zhou, D. Lai, H. Zhan and H. Chen, *J. Mater. Chem. C*, 2019, **7**, 10860–10867.
35 F. Gagnon, V. Tremblay, A. Soldera, M. U. Ocheje, S. Rondeau-Gagné, M. Leclerc and J.-F. Morin, *Mater. Adv.*, 2022, **3**, 599–603.
36 A. C. B. Rodrigues, A. Eckert, J. Pina, U. Scherf and J. S. Seixas de Melo, *Mater. Adv.*, 2021, **2**, 3736–3743.
37 C. Liu, X. Liu, G. Zheng, X. Gong, C. Yang, H. Liu, L. Zhang, C. L. Anderson, B. He, L. Xie, R. Zheng, H. Liang, Q. Zhou, Z. Zhang, J. Chen and Y. Liu, *J. Mater. Chem. A*, 2021, **9**, 23497–23505.
38 T. Bura, J. T. Blaskovits and M. Leclerc, *J. Am. Chem. Soc.*, 2016, **138**, 10056–10071.
39 A. L. Mayhugh, P. Yadav and C. K. Luscombe, *J. Am. Chem. Soc.*, 2022, **144**, 6123–6135.
40 H. Aoki, H. Saito, Y. Shimoyama, J. Kuwabara, T. Yasuda and T. Kanbara, *ACS Macro Lett.*, 2018, **7**, 90–94.
41 R. M. Pankow and B. C. Thompson, *Polym. Chem.*, 2020, **11**, 630–640.
42 Z. Ni, H. Wang, H. Dong, Y. Dang, Q. Zhao, X. Zhang and W. Hu, *Nat. Chem.*, 2019, **11**, 271–277.
43 Q. Wang, S. V. Lenjani, O. Dolynchuk, A. D. Scaccabarozzi, H. Komber, Y. Guo, F. Guenther, S. Gemming, R. Magerle, M. Caironi and M. Sommer, *Chem. Mater.*, 2021, **33**, 668–677.
44 Y. Liu, K. Xian, X. Zhang, M. Gao, Y. Shi, K. Zhou, Y. Deng, J. Hou, Y. Geng and L. Ye, *Macromolecules*, 2022, **55**, 3078–3086.
45 L. Giraud, S. Grelier, E. Grau, G. Hadziioannou, C. Brochon, H. Cramail and E. Cloutet, *J. Mater. Chem. C*, 2020, **8**, 9792–9810.
46 N. R. Kakde, H. J. Bharathkumar, B. A. Wavhal, A. Nikam, S. Patil, S. R. Dash, K. Vanka, K. Krishnamoorthy, A. Kulkarni and S. K. Asha, *J. Mater. Chem. C*, 2022, **10**, 13025–13039.
47 M. Mooney, A. Nyayachavadi and S. Rondeau-Gagné, *J. Mater. Chem. C*, 2020, **8**, 14645–14664.
48 M. Wakioka, S. Ishiki and F. Ozawa, *Macromolecules*, 2015, **48**, 8382–8388.
49 J. Kuwabara and T. Kanbara, *Bull. Chem. Soc. Jpn.*, 2019, **92**, 152–161.
50 M. Leclerc, S. Brassard and S. Beaupre, *Polym. J.*, 2020, **52**, 13–20.
51 G. Qian, X. Wang, S. Wang, Y. Zheng, S. Wang, W. Zhu and Y. Wang, *Chem. – Eur. J.*, 2019, **25**, 15401–15410.
52 R. S. Ashraf, A. J. Kronemeijer, D. I. James, H. Sirringhaus and I. McCulloch, *Chem. Commun.*, 2012, **48**, 3939–3941.
53 F. Wang, Y. Dai, W. Wang, H. Lu, L. Qiu, Y. Ding and G. Zhang, *Chem. Mater.*, 2018, **30**, 5451–5459.